On-sky demonstration of segment piston estimation using an infrared tip-tilt sensor

Marcos A. van Dam[a], Mahawa Cissé[b], and Antonin H. Bouchez[b]

[a]Flat Wavefronts, 21 Lascelles Street, Christchurch 8022, New Zealand
[b]W. M. Keck Observatory, 65-1120 Mamalahoa Highway, Kamuela, HI 96743

ABSTRACT

The Giant Magellan Telescope (GMT) consists of seven 8.365-m diameter circular segments in a petal pattern to create a telescope with an effective diameter of 25.4 m. The Laser Tomography Adaptive Optics system for the GMT uses six Shack-Hartmann Wavefront Sensors (SHWFSs) guiding on six laser guide stars to measure high-order wavefront aberrations. Because tip-tilt measurements are corrupted by uplink disturbances, they are measured using a natural guide star with an infrared tip-tilt sensor operating at 500 Hz. Segment piston induced by the atmosphere or the telescope is invisible to the SHWFSs. In previous work, we demonstrated through numerical simulations that segment piston can be recovered from tip-tilt sensor images using phase retrieval. In this paper, we present the results of on-sky experiments using the W. M. Keck Observatory as a testbed for GMT segment piston sensing. Short-exposure, near infrared AO-corrected images were taken with the NIRC2 camera on Keck II. Segment piston was applied to three blocks of 12 contiguous segments to emulate the large segments of the GMT. The images were processed using a modified Gerchberg-Saxton phase retrieval algorithm and a non-linear optimization algorithm to recover the applied segment piston. The on-sky experiments confirm the suitability of phase retrieval to maintain telescope phasing for the GMT.

Keywords: Giant Magellan Telescope, Keck Observatory, segment phasing, adaptive optics, laser tomography adaptive optics, phase retrieval, Gerchberg-Saxton

1. INTRODUCTION

The Giant Magellan Telescope (GMT) consists of seven 8.365 m circular segments with a separation of 8.710 m between the central segment and the outer segments (Fig. 1). The GMT is a Gregorian design with an adaptive

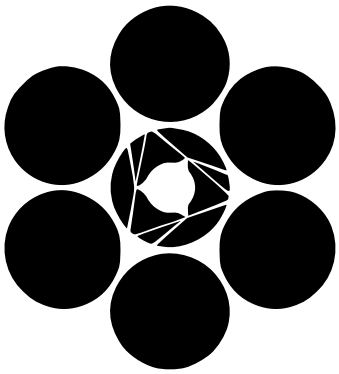

Figure 1: The GMT telescope pupil.

secondary mirror (ASM). The ASM is also segmented, with the segments critically sized with respect to the primary mirror segments. The design of the GMT is ideal for ground-layer adaptive optics, high contrast imaging and imaging at thermal infrared wavelengths.

Send correspondence to Marcos van Dam, e-mail: marcos@flatwavefronts.com

In order to form images at the diffraction limit of the telescope (equivalent to a diameter of approximately 25.4 m), it is crucial to phase the total optical path of each primary-secondary mirror pair to a small fraction of the imaging wavelength. The GMT has two diffraction-limited adaptive optics (AO) modes which require a phased telescope.[1] The natural guide star adaptive optics (NGAO) mode guiding on a visible light pyramid wavefront sensor is used when there is a sufficiently bright star within approximately 30″ from the science target. For greater sky coverage, there is also a laser tomography adaptive optics (LTAO) system that employs six side-projected laser guide stars (LGSs), along with a single natural guide star (NGS) used to measure tip-tilt. This tip-tilt star can be much fainter and further away from the science target than the guide star used in NGAO mode.

Two first generation instruments are fed LTAO-corrected wavefronts: the Giant Magellan Telescope Integral Field Spectrograph (GMTIFS)[2] and the Giant Magellan Telescope Near Infrared Spectrograph (GMTNIRS).[3] Each instrument is equipped with its own on-instrument wavefront sensor (OIWFS) that guides on an NGS. The OIWFS is required to make tip-tilt measurements at 500 Hz, focus measurements at 10 Hz and high-order truth measurements at 0.03 Hz in order to recover the modes that the laser tomography wavefront sensor (LTWS) is not able to measure. The tip-tilt sensor in the OIWFS consists of a Nyquist sampled imager operating at K-band (2.179 µm). The GMTNIRS OIWFS uses 5–10% of the light from the on-axis science target, with the remainder of the light sent to the spectrograph. GMTIFS uses a pick-off mirror to send all of the light from a guide star situated between 15″ and 90″ off-axis to the OIWFS. A dedicated deformable mirror (DM) is used to correct the high-order anisoplanatism in the direction of the tip-tilt star.

The motivation for this paper is most easily understood via inspection of Figure 2. Uncorrected phasing errors in the primary mirror segments of the GMT degrade the point spread function (PSF) of the science images. Figure 2 displays some simulated residual wavefronts, with and without the use of segment piston correction based on the tip-tilt sensor images, along with the corresponding PSFs.

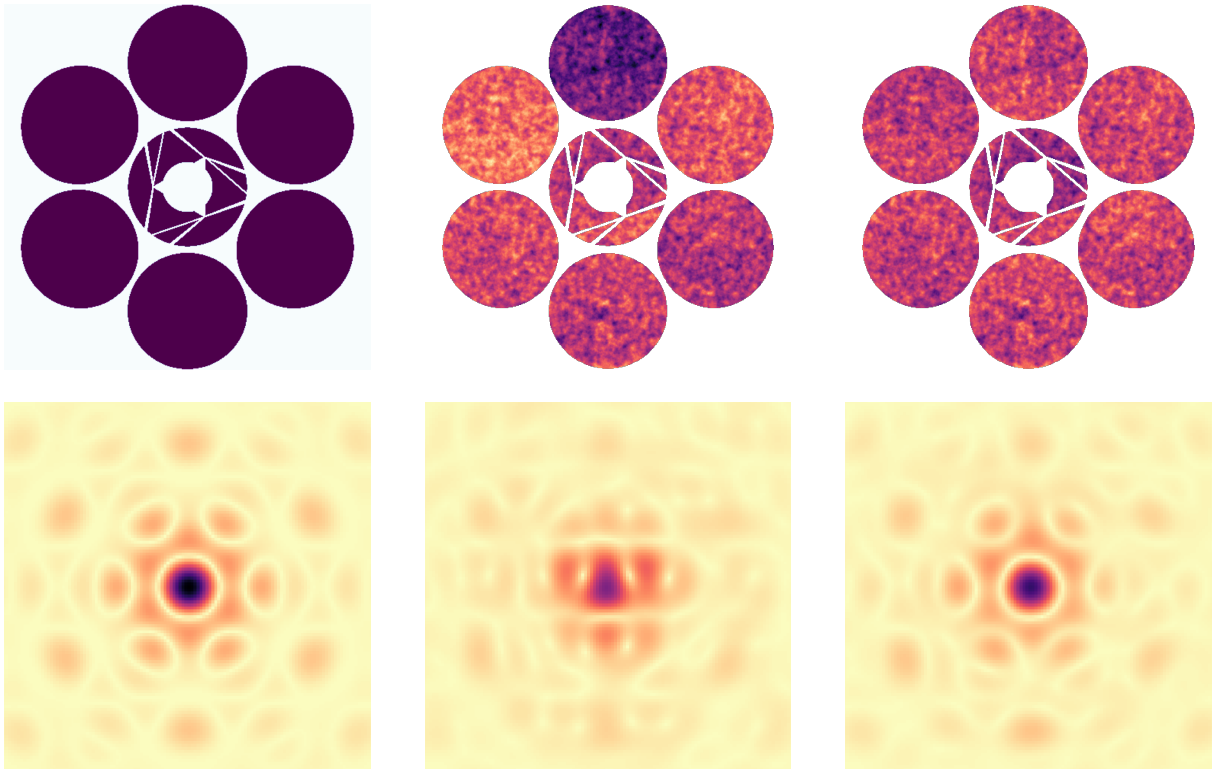

Figure 2: Wavefront errors (top) and corresponding PSF (bottom). Flat incoming wavefront (left), typical LTAO residual wavefront without (center) and with (right) segment piston control.

In previous work, we demonstrated through numerical simulations that segment piston can be sensed from tip-tilt sensing images using phase retrieval.[4] In this paper, we present the results of on-sky experiments using the Keck II telescope at the W. M. Keck Observatory ("Keck") as a testbed for GMT segment piston sensing. The segment phasing strategy for GMT in LTAO mode is described in van Dam *et al.*[4] and references therein.

The remainder of the paper is as follows. Section 2 describes how we use the Keck II telescope as a testbed for measuring segment piston similar to those encountered by the GMT. The phase retrieval algorithms used in this work are presented in Section 3. The analysis of on-sky images from three nights of experiments are reported in Section 4. Finally, conclusions are drawn in Section 5.

2. EXPERIMENTAL SETUP USING THE KECK II AO SYSTEM AND NIRC2

The W. M. Keck Observatory consists of two almost identical telescopes situated on the summit of Maunakea, Hawaii, at an elevation of 4145 m. The primary mirror of each telescope has 36 hexagonal segments, and a gap between adjacent segments of the order of 3 mm. The distance between opposite vertices of the hexagon is 1.8 m, leading to an effective diameter of 10 m and a circumscribed diameter of 10.95 m. An image of the telescope pupil is shown in Figure 3. An important problem for the Keck telescopes is maintaining the alignment of the primary

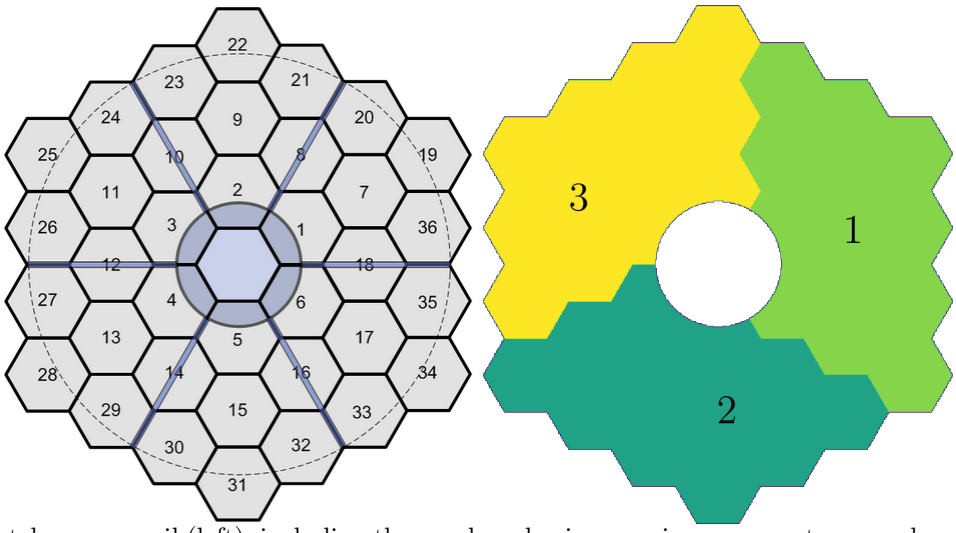

Figure 3: Keck telescope pupil (left), including the numbered primary mirror segments, secondary mirror central obscuration and the spiders. The dotted circle represents a circular aperture with a 9 m diameter. The figure on the right shows the segment groups used to emulate GMT segment piston.

mirror segments to ensure optimal image quality. The telescopes employ a dedicated phasing camera to measure segment piston across the segment gap.[5] Once the optimal segment positions have been found, capacitive sensors maintain the distance between adjacent segments. A large number of researchers have attempted various phase retrieval techniques on the Keck telescopes, with modest degrees of success, as described in van Dam et al (2015).[6] The last decade has seen a resurgence in the interest in improving the telescope phasing, with the implementation of a dedicated Zernike phase sensor on Keck II[7,8] and the deployment of the Fast & Furious (F&F) algorithm to remove static aberrations in the science images, whether they originate from segment piston errors or from other sources, such as calibration errors or evolving centroid gains.[9] It is important, however, to emphasize that the work here is entirely motivated by the desire to keep the GMT segments phased, and not to address the Keck phasing problem. The Keck segments are much smaller than the GMT segments, so we emulate the GMT segment piston by applying segment piston to contiguous blocks of 12 Keck primary mirror segments, as shown in Fig. 3.

At the time of the experiments, the Keck II AO system used a Shack-Hartmann wavefront sensor (SHWFS) with 20×20 subapertures across the telescope pupil with 2×2 pixels per subaperture to measure the wavefront aberrations. The wavefront slopes are reconstructed into DM commands and applied to a Xinetics 349 actuator

deformable mirror (DM).[10–13] At the start of 2026, the Keck II AO system was upgraded with a new 60×60 actuator ALPAO deformable mirror and a 57×57 subaperture WFS.[14]

The NIRC2 camera is a near-infrared imager and spectrograph that is fed by the Keck II AO system. It has a 1024×1024 pixel HgCdTe array with a pixel scale of 9.942 mas in the narrow camera mode. The Brackett Gamma filter, a narrowband filter with a central wavelength of 2.168 µm, was used. At this wavelength, 22 mas corresponds to Nyquist sampling. The images were taken in subarray mode, with the central 128×152 pixels read with an integration time of 11 ms and 100 coadds. Because every coadd is saved, each file contains 100 images.

3. PHASE RETRIEVAL ALGORITHMS

Phase retrieval is the term given to the process of deducing the phase of the complex amplitude of the electric field at the pupil plane based on a measurement at or near the focal plane. Two different iterative algorithms to measure segment piston from tip-tilt sensor images were proposed in van Dam *et al.*,:[4] the sequential Gerchberg-Saxton algorithm and the Fast & Furious algorithm. In this work, we are unable to use these algorithms because they rely on the application of a known segment piston command between successive images. Instead, we use a modified implementation of the well-known Gerchberg-Saxton (G-S) algorithm,[15,16] and a non-linear fit of segment piston and low-order modes to the images. Our baseline algorithm for the GMT is the Fast & Furious algorithm,[17,18] which has already found application in astronomical AO systems, but not for correcting segment piston. The implementation of the G-S and F&F algorithms has been made freely available as a Python package named *pripy*.[19]

3.1 Preprocessing steps

Some preprocessing of the images is required before unleashing the Gerchberg-Saxton algorithm or the non-linear fit:

(i) Extract a region of the image centered around the location of the tip-tilt star.

(ii) Recenter the image using FFT interpolation so it is centered as well as possible.

(iii) Threshold the pixel values to zero.

Recentering the image removes the mean tip-tilt in the phase, a term which we do not want to measure and reduces the dynamic range of the G-S algorithm.

3.2 Gerchberg-Saxton algorithm

The Gerchberg-Saxton algorithm has a history spanning half a century since the seminal paper by Gerchberg and Saxton.[15] It consists of a very simple non-linear iterative algorithm that solves for the phase at the pupil plane based on knowledge about the amplitude at the pupil plane, $A_0(x, y)$, and a measurement of the amplitude at the image plane, $a_0(u, v)$, which is the square root of the measured image. The initial guess for the phase in the pupil plane, $\phi(x, y)$ usually consists of random pixel values uniformly distributed between $-\pi$ and π radians. For successive images, we have the option to begin with the phase estimate corresponding to the previous image (*i.e.*, a "warm start"), but this did not appear to reduce the convergence time. The complex amplitude at the pupil plane, $A_0(x, y) \exp[i\phi(x, y)]$, is used to compute the corresponding complex amplitude at the image plane, $a \exp[i\psi(u, v)]$. In what follows we drop the coordinates (x, y) and (u, v) for clarity. We write

$$a \exp[i\psi] = \mathcal{F}[A_0 \exp[i\phi]]. \tag{1}$$

where ψ represents the phase at the image plane and $\mathcal{F}$ represents the Fourier transform, computed using the Fast Fourier Transform (FFT) algorithm. The measured amplitude at the focal plane, a_0, replaces the calculated value, a, and the complex amplitude at the pupil plane is recomputed:

$$A \exp[i\phi] = \mathcal{F}^{-1}[a_0 \exp[i\psi]], \tag{2}$$

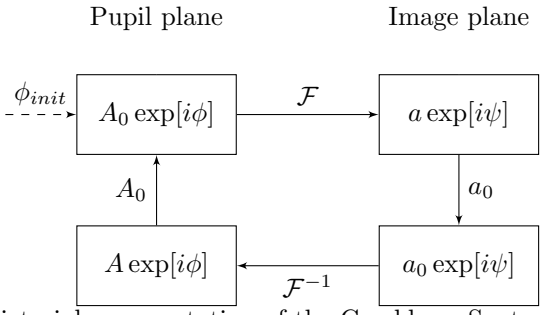

Figure 4: Pictorial representation of the Gerchberg-Saxton algorithm.

where $\mathcal{F}^{-1}$ denotes the inverse Fourier transform. The measured pupil amplitude, A_0, replaces the calculated amplitude, A, and the procedure iterates between Eq. (1) and Eq. (2), as depicted by Figure 4.

The Gerchberg-Saxton algorithm has the desirable property that its error metric is non-increasing, and has been shown to be a steepest-descent algorithm.[16] Unfortunately, it can stagnate (*i.e.*, converge to a local minimum) or converge to a phase-wrapped solution. In order to speed up the convergence and to reduce the possibility of converging to a local minimum, two modifications are made for the first 10 iterations of the algorithm. First, the amplitude of the image outside of the valid region where the signal-to-noise (SNR) ratio is high is forced to be zero: *i.e.*,

$$a_0(u,v) = \begin{cases} a_0(u,v), & \text{if } |u| \leq d \text{ and } |v| \leq d \\ 0, & \text{otherwise} \end{cases} \tag{3}$$

where d is the half of valid support. Driving the amplitude to zero outside the central region of the image improves the speed of convergence but introduces artefacts in the reconstructed phase. Second, the modifications known as the hybrid input-output algorithm are made. The equations Eq. (1) and Eq. (2) are replaced by:

$$a \exp[i\psi] = \mathcal{F}[(A_0 + h(A_0 - A)) \exp[i\phi]], \tag{4}$$

and

$$A \exp[i\phi] = \mathcal{F}^{-1}[(a_0 + h(a_0 - a)) \exp[i\psi]]. \tag{5}$$

where h is a constant with a typical value of 0.3. After 10 iterations, the value of h is set to 0 and the algorithm resumes for 10 more iterations. However, the image pixels outside the valid support are no longer forced to zero, but are allowed to "float": *i.e.*,

$$a_0(u,v) = \begin{cases} a_0(u,v), & \text{if } |u| \leq d \text{ and } |v| \leq d \\ a(u,v), & \text{otherwise} \end{cases} \tag{6}$$

This step greatly reduces the level of artefacts in the reconstructed phase. This approach is similar to what is proposed in Fienup (1993), where a weighting is applied to the pixels in the image plane.[20]

The solution obtained by any phase retrieval based on a single image is not unique, as there are three changes that can be made to the phase that do not affect the amplitude at the focal plane:[21]

- Addition of a constant to $\phi(x,y)$.
- Addition of a multiple of 2π to any point in $\phi(x,y)$ for monochromatic light.
- Replacing $\phi(x,y)$ by $-\phi(-x,-y)$ if $A(x,y)$ is symmetrical.

The first point refers to the well-known fact that global piston does not affect the image. The second point leads to the possibility of phase wrapping, where there are discontinuous jumps of 2π radians in the solution. This

is detected and resolved if necessary using phase unwrapping. Finally, the so-called phase ambiguity problem arises for symmetrical pupils, where there are two solutions that are consistent with the measured intensity. The phase ambiguity was resolved by knowledge of the sign of a small defocus in the images.

The resulting wavefront was decomposed into five modes: global tip-tilt, and three segment piston modes.

3.3 Non-linear fit of segment piston and low-order modes

A non-linear optimization was used to find the value of six modes: tip and tilt, focus, and piston values for segments one, two and three. Since global piston is constrained to be zero, there are only two independent segment piston modes, leaving five modes in total. A set of five orthonormal modes was created using Gram-Schmidt orthonormalization. The five orthonormal modes are displayed in Fig. 5. A Nelder-Mead non-linear search was run to find the value of the five modes that minimizes the squared difference between the measured and modeled image intensities.

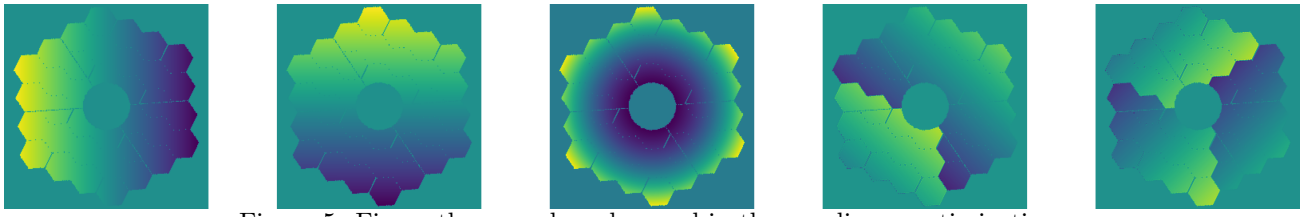

Figure 5: Five orthonormal modes used in the non-linear optimization.

3.4 Numerical experiments using simulated data

Before attempting to process the on-sky data, it is instructive to process simulated data in the same way. A wavefront map with segment piston was generated and used to compute the PSF. The applied segment piston was 55 nm, −140 nm and 85 nm, to be consistent with one of the on-sky experiments. The Gerchberg-Saxton algorithm was run, and produced the two equally valid solutions, shown in Fig. 6. While the wavefront has an RMS value of 100 nm, much of the power in the segment piston can be removed by subtracting global tip-tilt from the wavefront. The tip-tilt removed wavefront has an RMS value of only 61 nm.

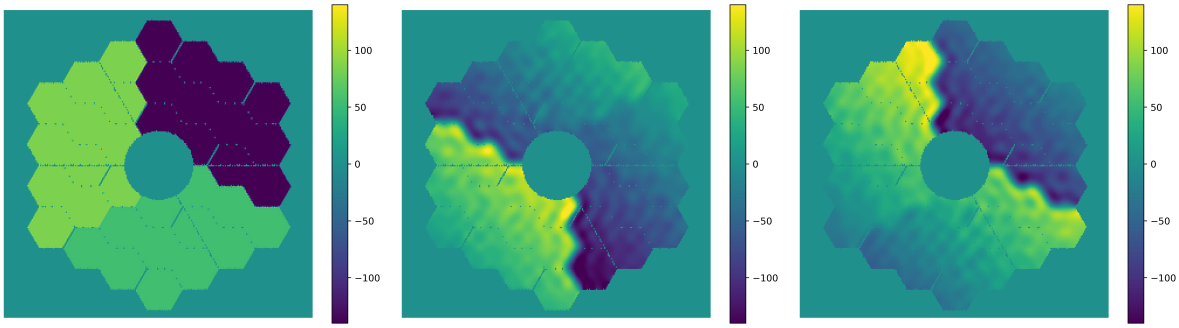

Figure 6: Applied segment piston in the simulation (left) and the two possible reconstructed wavefronts (center and right). The applied segment piston was [55, -140, 85] nm.

4. EXPERIMENTAL ON-SKY RESULTS

In this section, we report the results of the on-sky experiments where segment piston is applied to the telescope and the phase is recovered using phase retrieval. Data was taken on three separate nights. The dates reported in this paper are Universal Time (UT).

4.1 Data set taken on 3 December 2025

A defocus was applied to determine which of the two solutions produced by the phase retrieval algorithms is the correct one. All of the data on this night was taken with the science camera out of focus by 1.08 mm, which corresponds to an RMS wavefront error of approximately 170 nm for a 10 m-diameter circular aperture.

The first data set was taken with the primary mirror segments sent to the nominal telescope phasing values determined by the phasing camera system (PCS). The second set applied offsets of [27, 106, -133] nm to the M1 segments, while a third set applied [-239, 318, -79] nm, as tabulated in Table 1. Twenty NIRC2 images were taken for each segment piston configuration with 100 coadds per image. Each coadd can be extracted from the image and processed independently. It is not possible to measure the Strehl ratio of the images accurately because the field of view is insufficient to estimate the photometry. However, the relative Strehl ratio was estimated by first upsampling the images using FFT interpolation and then finding the subpixel peak of the upsampled images.

Data Set	Segment 1	Segment 2	Segment 3	Image peak
1	0	0	0	233515
2	27	106	-133	226616
3	-239	318	-79	181129

Table 1: Data set, applied segment piston and average peak value.

Typical short-exposure images from the three data sets are shown in Fig. 7. The change in the PSF is clearly visible as segment piston is applied to the primary mirror.

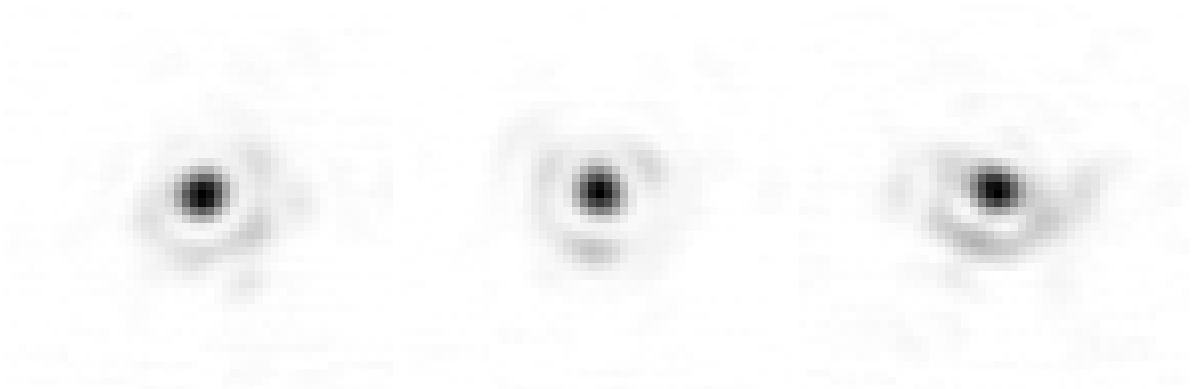

Figure 7: Representative short-exposure images from Data Sets 1, 2 and 3.

It is striking that the Strehl ratio drops by so little when 99 nm of segment piston is applied. This was investigated further using numerical simulations in YAO.[22] The simulation results, presented in Table 2, show that there is only a small drop in Strehl ratio when 99 nm of segment piston are applied, which is consistent with the on-sky findings. However, larger phasing error leads to a more significant drop in Strehl ratio.

	Phasing error		
	0 nm	99 nm	234 nm
On-sky	1.000	0.970	0.776
Simulations without turbulence	1.000	0.978	0.740
Simulations with turbulence	1.000	0.984	0.729

Table 2: Reduction in Strehl ratio from the on-sky measurements and from simulations.

Figure 8 shows graphically that the adaptive optics system is able to measure and partially compensate for segment piston errors provided that these errors are sufficiently small. It is generally believed that Shack-

Hartmann wavefront sensors are insensitive to segment piston errors, but this is not entirely true: discontinuities in the wavefront can be measured provided that they are sufficiently small relative to the wavelength.

Figure 8: Simulated residual wavefront (nm) when applying 99 nm RMS of segment piston with the adaptive optics loop open (left) and closed (right). No other disturbances are present.

Two algorithms were used to estimate segment piston: the Gerchberg-Saxton algorithm and a non-linear optimization that estimates five modes. After convergence of the Gerchberg-Saxton algorithm, phase wrapping was sometimes observed in the solution. The phase was unwrapped using the Python package *unwrap*[23] and then converted to a wavefront. Due to phase ambiguity, there are two possible solutions. The solution with a positive focus was selected to be the correct solution. The applied focus was then removed, along with any residual tip-tilt and global piston. This wavefront was used to estimate the three segment piston values.

Figure 9 plots the segment piston values for each of the 100 coadds from the first image of Data Set 3. The

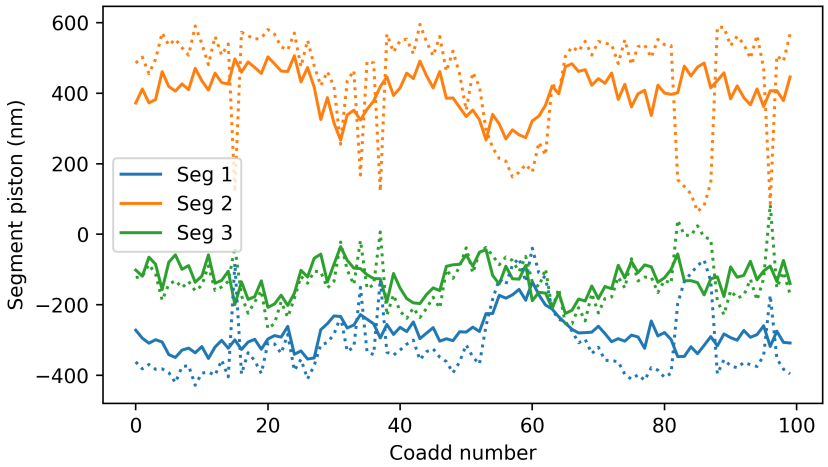

Figure 9: Estimated segment piston for each coadd using the Gerchberg-Saxton algorithm (solid) and the non-linear optimization (dotted) from the first image of Data Set 3.

segment piston estimates are consistent from frame to frame, and generally agree between the two methods, although the non-linear optimization has a larger variation from frame to frame. Some of the variation in the segment piston estimates is likely to be caused by uncorrected turbulence or changes in the centroid gain, which leads to biases in the centroid measurements of the WFS. The focus estimate was always between 110 nm and 180 nm when using the Gerchberg-Saxton algorithm, clearly showing that the images were sufficiently defocused to resolve the phase ambiguity.

The same analysis is applied to all 60 image files. For each file, we compute the segment piston for each coadd and average the results over all 100 coadds.

The segment piston values averaged over every file are tabulated in Table 3. The analysis was repeated using images integrated over 100 coadds, and these results are recorded in the last three rows. As expected, short

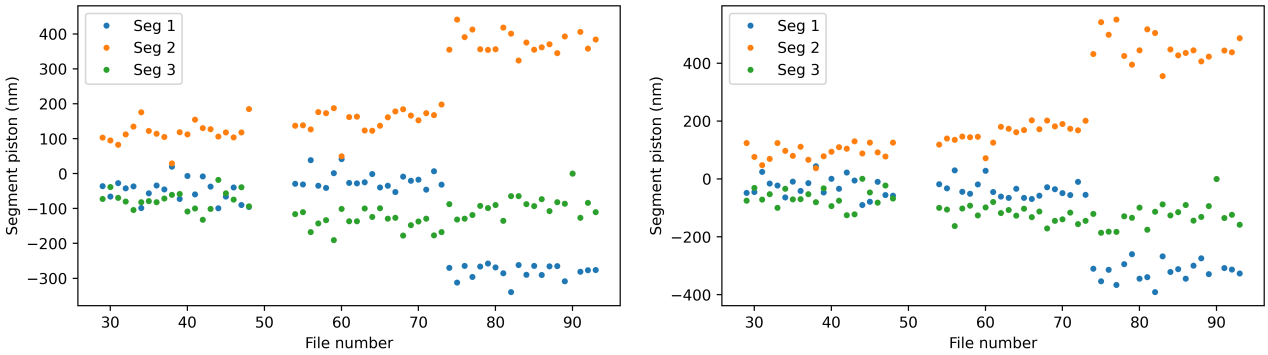

Figure 10: Mean estimated segment piston for each file using the Gerchberg-Saxton algorithm (left) and the non-linear optimization (right). There are 20 consecutive images corresponding to, from left to right, Data Sets 1, 2 and 3.

exposures produce more reliable segment piston estimates.

		Applied piston			Gerchberg-Saxton			Non-linear optimization		
Data Set	Integrated	Seg. 1	Seg. 2	Seg. 3	Seg. 1	Seg. 2	Seg. 3	Seg. 1	Seg. 2	Seg. 3
1	No	0	0	0	-50	117	-76	-27	93	-65
2	No	27	106	-133	-19	154	-137	-37	160	-122
3	No	-239	318	-79	-267	358	-93	-303	431	-126
1	Yes	0	0	0	-54	228	-175	-19	70	-51
2	Yes	27	106	-133	-26	235	-209	-23	119	-94
3	Yes	-239	318	-79	-286	395	-111	-291	393	-101

Table 3: Segment piston values averaged over every file in each data set. The first three rows apply phase retrieval to each coadd and then average, while the next three rows integrate the images and then retrieve the phase.

An alternative way to visualize the data is to compare the difference in segment piston, rather than the absolute value (Table 4). Both methods produce consistent reconstructions, with the non-linear optimization outperforming the Gerchberg-Saxton reconstruction for this data set. The applied segment piston is slightly underestimated using the Gerchberg-Saxton algorithm. There are two reasons for this. First, as we saw earlier, the adaptive optics partly compensates for the applied segment piston when the applied segment piston is small. This problem will not occur when using the LTAO system at GMT, both because the segment gaps are large and because there is no evidence that the wavefront sensor can measure segment piston when guiding on an LGS. Second, it is well-known that the estimates produced by the Gerchberg-Saxton algorithm are biased towards zero. In closed-loop operation, this will not be an issue as the segment piston will be compensated in an iterative manner.

	Applied piston			Gerchberg-Saxton			Non-linear optimization		
Data Set	Seg. 1	Seg. 2	Seg. 3	Seg. 1	Seg. 2	Seg. 3	Seg. 1	Seg. 2	Seg. 3
2 minus 1	27	106	-133	31	37	-61	-10	67	-57
3 minus 1	-239	318	-79	-217	241	-17	-276	338	-61

Table 4: Difference in estimated segment piston values averaged over every file in each data set obtained by retrieving the phase from each coadd and then averaging.

4.2 Data set taken on 8 December 2025

A similar data set was taken on 8 December 2025. This time, the images were defocused by 0.6 mm, corresponding to a wavefront error of 96 nm RMS. The images were taken first with the best segment piston map as measured by the PCS. To this phase map, the offsets of [27, 106, -133] nm and [-266, 212, 54] nm were added.

Table 5 shows that the Gerchberg-Saxton reconstruction produces the most accurate results. As expected, the change in segment piston is underestimated for the case where only 99 nm RMS of segment piston is applied, because the AO system partially compensates for the applied segment piston.

	Applied piston			Gerchberg-Saxton			Non-linear optimization		
Data Set	Seg. 1	Seg. 2	Seg. 3	Seg. 1	Seg. 2	Seg. 3	Seg. 1	Seg. 2	Seg. 3
2 minus 1	27	106	-133	20	91	-103	1	60	-60
3 minus 1	-266	212	54	-264	192	81	-193	128	63

Table 5: Difference in estimated segment piston values averaged over every file in each data set obtained by retrieving the phase from each coadd and then averaging.

4.3 Data set taken on 5 October 2025

The original data set, taken on 5 October 2025, used in-focus measurements only. The images were taken with the best segment piston map as measured by the PCS, and then with the same segment piston offset of [55, -140, 85] nm. Using the defocused data sets, we have learned to convert wavefront reconstructions into segment piston measurements. For the data where the segments are poked, we know the reconstructed segment piston that we expect and can use the Gerchberg-Saxton solution that matches the sign of the expected segment piston. The results, shown in Table 6, show excellent agreement between the applied and the reconstructed segment piston. The non-linear optimization procedure was not used on this data set.

	Applied piston			Gerchberg-Saxton		
Data Set	Seg. 1	Seg. 2	Seg. 3	Seg. 1	Seg. 2	Seg. 3
2 minus 1	55	-140	85	67	-136	61

Table 6: Difference in estimated segment piston values averaged over every file in each data set obtained by retrieving the phase from each coadd and then averaging.

5. CONCLUSION AND DISCUSSION

The GMT plans to use phase retrieval to measure segment piston errors using short exposure K-band images from the tip-tilt sensor when operating in LTAO mode. In this paper, we present the results of on-sky experiments using the Keck II telescope as a testbed. Known segment piston offsets were applied to three blocks of 12 contiguous primary-mirror segments and subsequently recovered using phase retrieval. The applied segment piston is clearly visible in the images. It was found both from simulations and the on-sky data that the NGS WFS is able to partially compensate for segment piston errors when the applied segment piston is of the order of 100 nm (well under half a wave at the wavefront sensing wavelength). For this reason, we are unable to determine the limiting accuracy of the phase retrieval algorithms. When larger segment piston errors are applied, phase retrieval produces segment piston estimates that are consistent with the applied values. In future work, two modifications to the experiment could be made. The first is to make the measurements in LGS AO mode, a wavefront sensing mode that is expected to be blind to segment piston errors. The second is to close the loop by converting the segment piston values into M1 segment piston commands and applying them to the telescope. Operating iteratively would allow the use of the Fast & Furious algorithm and also to quantify the limits of performance of phase retrieval for segment piston estimation.

Acknowledgement

The W. M. Keck Observatory is operated as a scientific partnership among the California Institute of Technology, the University of California, and the National Aeronautics and Space Administration. The Observatory was made possible by the generous financial support of the W. M. Keck Foundation. The authors wish to recognize and acknowledge the very significant cultural role and reverence that the summit of Maunakea has always had within the indigenous Hawaiian community. We are most fortunate to have the opportunity to conduct observations from this mountain.

REFERENCES

[1] Bouchez, A. H., Acton, D. S., Biasi, R., Conan, R., Espeland, B., Esposito, S., Filgueira, J., Gallieni, D., McLeod, B. A., Pinna, E., et al., "The Giant Magellan Telescope adaptive optics program," in [*Adaptive Optics Systems IV*], **9148**, 300–318, SPIE (2014).

[2] Sharp, R., Adams, D., Bloxham, G., Boz, R., Bundy, D., Chandler, D., Gausachs, G., Gers, L., Hart, J., Herrald, N., et al., "Design evolution of the Giant Magellan Telescope integral field spectrograph, GMTIFS," in [*Ground-based and Airborne Instrumentation for Astronomy VII*], **10702**, 597–608, SPIE (2018).

[3] Jaffe, D. T., Barnes, S., Brooks, C., Lee, H., Mace, G., Pak, S., Park, B.-G., and Park, C., "GMTNIRS: progress toward the Giant Magellan Telescope near-infrared spectrograph," in [*Ground-based and Airborne Instrumentation for Astronomy VI*], **9908**, 648–656, SPIE (2016).

[4] van Dam, M. A., Cranney, J., and Bouchez, A., "Segment piston estimation using sequential phase retrieval," in [*Adaptive Optics for Extremely Large Telescopes 7th Edition*], (2023).

[5] Chanan, G., Troy, M., Dekens, F., Michaels, S., Nelson, J., Mast, T., and Kirkman, D., "Phasing the mirror segments of the keck telescopes: the broadband phasing algorithm," *Applied optics* **37**(1), 140–155 (1998).

[6] van Dam, M. A., Ragland, S., and Wizinowich, P. L., "Effect of segmented telescope phasing errors on adaptive optics performance," *Adaptive Optics for Extremely Large Telescopes 4th Edition* (2015).

[7] Salama, M., Guthery, C., Chambouleyron, V., Jensen-Clem, R., Wallace, J. K., Delorme, J.-R., Troy, M., Wenger, T., Echeverri, D., Finnerty, L., et al., "Keck primary mirror closed-loop segment control using a vector-zernike wavefront sensor," *The Astrophysical Journal* **967**(2), 171 (2024).

[8] Salama, M., Cissé, M., Chambouleyron, V., Guthery, C., Jensen-Clem, R., Wallace, J. K., Troy, M., Pueyo, L., Bouchez, A., Echeverri, D., et al., "Analyzing the zernike wavefront sensor closed-loop segment cophasing performance on keck so far," in [*Techniques and Instrumentation for Detection of Exoplanets XII*], **13627**, 135–150, SPIE (2025).

[9] Guthery, C., Bottom, M., Bouchez, A., Delorme, J., Karkar, S., Richards, P., and Wizinowich, P., "Optimizing keck adaptive optics: correcting residual errors with focal-plane wavefront sensing," in [*Adaptive Optics Systems IX*], **13097**, 130975Y, SPIE (2024).

[10] Johansson, E. M., van Dam, M. A., Stomski, P. J., Bell, J. M., Chin, J. C., Sumner, R. C., Wizinowich, P. L., Biasi, R., Andrighettoni, M., and Pescoller, D., "Upgrading the keck ao wavefront controllers," in [*Adaptive Optics Systems*], **7015**, 955–966, SPIE (2008).

[11] van Dam, M. A., Le Mignant, D., and Macintosh, B. A., "Performance of the keck observatory adaptive-optics system," *Applied Optics* **43**(29), 5458–5467 (2004).

[12] Wizinowich, P. L., Le Mignant, D., Bouchez, A. H., Campbell, R. D., Chin, J. C., Contos, A. R., van Dam, M. A., Hartman, S. K., Johansson, E. M., Lafon, R. E., et al., "The wm keck observatory laser guide star adaptive optics system: overview," *Publications of the Astronomical Society of the Pacific* **118**(840), 297–309 (2006).

[13] van Dam, M. A., Bouchez, A. H., Le Mignant, D., Johansson, E. M., Wizinowich, P. L., Campbell, R. D., Chin, J. C., Hartman, S. K., Lafon, R. E., Stomski Jr, P. J., et al., "The wm keck observatory laser guide star adaptive optics system: performance characterization," *Publications of the Astronomical Society of the Pacific* **118**(840), 310–318 (2006).

[14] Guthery, C. E., Taylor, J., Lilley, S., Marin, E., Vincent, M., Jensen-Clem, R., Cetre, S., Salama, M., Steiner, J., Umiamaka, T., Wetherell, E., Wizinowich, P., and Bouchez, A., "First on-sky results of the haka deformable mirror upgrade," in [*Adaptive Optics Systems X*], Jackson, K. J., Schmidt, D., and Vernet, E., eds., **14150**, International Society for Optics and Photonics, SPIE (2026).

[15] Gerchberg, R. W. and Saxton, W. O., "A practical algorithm for the determination of the phase from 1057 image and diffraction pictures," *Optik* **35**(237–246), 237–246 (1972).

[16] Fienup, J. R., "Phase retrieval algorithms: a comparison," *Appl. Opt.* **21**, 2758–2769 (Aug 1982).

[17] Korkiakoski, V., Keller, C. U., Doelman, N., Kenworthy, M., Otten, G., and Verhaegen, M., "Fast & furious focal-plane wavefront sensing," *Appl. Opt.* **53**(20), 4565–4579 (2014).

[18] Bos, S. P., Vievard, S., Wilby, M. J., Snik, F., Lozi, J., Guyon, O., Norris, B. R. M., Jovanovic, N., Martinache, F., Sauvage, J.-F., and Keller, C. U., "On-sky verification of Fast and Furious focal-plane wavefront sensing: moving forward toward controlling the island effect at Subaru/SCExAO," *A&A* **639**, A52 (2020).

[19] Cranney, J., "Phase Retrieval In PYthon." https://github.com/jcranney/pripy (2022).

[20] Fienup, J. R., "Phase-retrieval algorithms for a complicated optical system," *Applied optics* **32**(10), 1737–1746 (1993).

[21] Lane, R., Fright, W., and Bates, R., "Direct phase retrieval," *IEEE transactions on acoustics, speech, and signal processing* **35**(4), 520–526 (1987).

[22] Rigaut, F. and van Dam, M. A., "Simulating astronomical adaptive optics systems using yao," *Adaptive Optics for Extremely Large Telescopes 3rd Edition* (2013).

[23] Herráez, M. A., Burton, D. R., Lalor, M. J., and Gdeisat, M. A., "Fast two-dimensional phase-unwrapping algorithm based on sorting by reliability following a noncontinuous path," *Applied optics* **41**(35), 7437–7444 (2002).